

Spectrally recycling space-time wave packets

Layton A. Hall¹ and Ayman F. Abouraddy¹

¹CREOL, The College of Optics & Photonics, University of Central Florida, Orlando, FL 32816, USA

‘Space-time’ (ST) wave packets are propagation-invariant pulsed optical beams that travel rigidly in linear media without diffraction or dispersion at a potentially arbitrary group velocity. These unique characteristics are a result of spatio-temporal spectral correlations introduced into the field; specifically, each spatial frequency is associated with a single temporal frequency (or wavelength). Consequently, the spatial and temporal bandwidths of ST wave packets are correlated, so that exploiting an optical source with a large temporal bandwidth or achieving an ultralow group velocity necessitate an exorbitantly large numerical aperture. Here we show that ‘spectral recycling’ can help overcome these challenges. ‘Recycling’ or ‘reusing’ each spatial frequency by associating it with multiple distinct but widely separated temporal frequencies allows one to circumvent the proportionality between the spatial and temporal bandwidths of ST wave packets, which has been one of their permanent characteristics since their inception. We demonstrate experimentally that the propagation invariance, maximum propagation distance, and group velocity of ST wave packets are unaffected by spectral recycling. We also synthesize a ST wave packet with group velocity $c/14.3$ (c is the speed of light in vacuum) with a reasonable numerical aperture made possible by spectral recycling.

I. INTRODUCTION

Since Brittingham discovered in 1983 a propagation-invariant (diffraction-free and dispersion-free) pulsed optical beam [1], a host of other wave packets that share this feature have been identified [2–10]. Such pulsed beams have been recently dubbed generically ‘space-time’ (ST) wave packets, because their propagation invariance is undergirded by tight spectral associations between the spatial and temporal degrees of freedom [11–18]. Specifically, each spatial frequency underlying the spatial profile of a ST wave packet is assigned to a single temporal frequency (or wavelength) underlying its temporal profile [19–21]. Nevertheless, exploiting the unique characteristics predicted theoretically for such propagation-invariant wave packets (such as arbitrary group velocities in free space [22–29]) has been hampered in practice by the lack of a precise methodology for spatio-temporal wave-packet synthesis [9]. Recently, a new strategy based on spatio-temporal spectral-phase modulation [30, 31] is now helping realize the full potential of ST wave packets. This technique has enabled demonstrations of arbitrary group velocities in free space [32, 33], transparent dielectrics [34, 35], planar waveguides [36], and plasmonic interfaces [37], accelerating wave packets [38], non-accelerating Airy wave packets [39], self-healing [40], novel ST Talbot effects [41], and even realizations using incoherent light [42, 43].

Nevertheless, a fundamental constraint is imposed on ST wave packets because the tight spatio-temporal spectral correlations entail a *proportionality* between the spatial and temporal bandwidths. Such a proportionality is absent from traditional pulsed optical beams in which the spatial and temporal degrees of freedom are more-or-less independent; that is, the spatial beam profile and the temporal pulse linewidth can be manipulated independently. In general, ultrashort optical pulses need not require large numerical apertures. For ST wave packets, on

the other hand, the proportionality between the spatial and temporal bandwidths entails that exploiting a large temporal bandwidth will exact a high price in terms of system design: a large spatial bandwidth – and thus high numerical aperture – is necessary. In general, the temporal bandwidth $\Delta\omega$ and the spatial bandwidth Δk_x (in one dimension) are related through $\Delta\omega \propto (\Delta k_x)^2$ [11, 30]. This proportionality is particularly exacerbating for ultraslow ST wave packets (group velocity $\tilde{v} \ll c$, where c is the speed of light in vacuum) [33]. Indeed, this bandwidth restriction has been a permanent feature of ST wave packets since their introduction into optical physics. Although progress has been made in exploiting larger temporal bandwidths by relying on lithographically inscribed phase plates [44, 45], the limit on lithographic spatial resolution is nevertheless quickly reached with increased bandwidths. Consequently, this constraint sets upper limits for the practically utilizable light-source bandwidth and the minimally achievable group velocity in free space.

Here we show that the proportionality between spatial and temporal bandwidths that is intrinsic to all propagation-invariant ST wave packets can be circumscribed *without* negative impact on any of their unique characteristics, thus paving the way to reducing the numerical aperture necessary for accommodating large temporal bandwidths and enabling the synthesis of ultraslow pulses in free space. Our strategy relies on spectral ‘recycling’; that is, each spatial frequency is recycled (or reused) N times in association with distinct but widely separated temporal frequencies, rather than used only once as is the case in typical ST wave packets. Consequently, the temporal spectrum can be increased – in principle, indefinitely – while retaining a *fixed* spatial bandwidth. In this approach, the full temporal bandwidth $\Delta\omega$ is divided into N sub-bandwidths $\Delta\omega_n$, $n=1, 2, \dots, N$, each associated with a *fixed* spatial bandwidth that is reduced by a factor $\sim \sqrt{N}$ with respect

to its non-recycled counterpart having the same temporal bandwidth. Although the spatio-temporal profile of the spectrally recycled ST wave packet exhibits an additional discrete structure, it nevertheless retains all the essential characteristics of its non-recycled counterpart: it is propagation-invariant and has the same group velocity. We experimentally verify this strategy using N up to 16, which has enabled the realization of ST wave packets with group velocity down to $\tilde{v} = c/14.3$ in free space at the same numerical aperture as that of a non-recycled ST wave packet with $\tilde{v} = c/2$. These results indicate the possibility of reaching ultralow group velocities in free space, and exploiting new sources of light in synthesizing ST wave packets and fields, such as supercontinuum laser sources, white light sources, and potentially even attosecond pulses.

II. THEORY OF SPECTRAL RECYCLING

We start our analysis from a traditional optical wave packet $E(x, z; t) = e^{i(k_0 z - \omega_0 t)} \psi(x, z; t)$ and express its envelope $\psi(x, z; t)$ in terms of an angular spectrum:

$$\psi(x, z; t) = \iint dk_x d\Omega \tilde{\psi}(k_x, \Omega) e^{ik_x x} e^{i(k_z - k_0)z} e^{-i\Omega t}, \quad (1)$$

where $\tilde{\psi}(k_x, \Omega)$ is the spatio-temporal spectrum, $\Omega = \omega - \omega_0$ is the temporal frequency with respect to the carrier frequency ω_0 , $k_0 = \frac{\omega_0}{c}$, k_x (the spatial frequency) is the transverse component and k_z is the longitudinal component of the wave vector along the transverse x and axial z coordinates, respectively. For simplicity, we consider the field to be uniform along y ($k_y = 0$). The spectral support domain of this pulsed beam is a two-dimensional patch on the surface of the light-cone $k_x^2 + k_z^2 = (\frac{\omega}{c})^2$ [30, 31]. In contrast, the spatio-temporal spectrum of a propagation-invariant ST wave packet [Fig. 1(a)] lies at the intersection of the light-cone with the spectral plane

$$\Omega = (k_z - k_0)c \tan \theta, \quad (2)$$

where the spectral tilt angle θ is measured with respect to the k_z -axis [30, 46]; see Fig. 1(a)-i. Consequently, each spatial frequency k_x is associated with a single temporal frequency Ω , $\tilde{\psi}(k_x, \Omega) \rightarrow \tilde{\psi}(k_x) \delta(\Omega - \Omega(k_x))$, where $\Omega(k_x)$ is the conic section at the intersection of the spectral plane with the light-cone [Fig. 1(a)-ii]. The envelope of the ST wave packet takes the form:

$$\psi(x, z; t) = \int dk_x \tilde{\psi}(k_x) e^{ik_x x} e^{-i\Omega(t - z/\tilde{v})} = \psi(x, 0; t - z/\tilde{v}), \quad (3)$$

which corresponds to a propagation-invariant wave packet that propagates rigidly in free space at a group velocity $\tilde{v} = c \tan \theta$ [22, 32]. Therefore, tuning θ changes \tilde{v} in free space above or below c (without violating relativistic causality [33, 46–49]). According to this construction, higher ω is associated with lower k_x when $\theta < 45^\circ$, and

with higher k_x otherwise. Because the spectral projection onto the $(k_z, \frac{\omega}{c})$ -plane in Fig. 1(a)-iii is a straight line, the wave packet propagates at a well-defined group velocity $\tilde{v} = c \tan \theta$ without group velocity dispersion (GVD) [50]. Increased deviation of the spectral projection onto the $(k_z, \frac{\omega}{c})$ -plane away from the light-line $k_z = \frac{\omega}{c}$ [Fig. 1(a)-iii] is associated with higher k_x [Fig. 1(a)-ii].

Finally, the spatio-temporal intensity profile $I(x, z; t)$ at a fixed axial plane z is shown in Fig. 1(a)-iv, which exhibits a characteristic X-shape [2, 33]. The pulse width $\Delta\tau$ at the beam center, defined as the width of $I(0, z; t)$ [Fig. 1(a)-iv], is the inverse of the temporal bandwidth $\Delta\omega$. The beam width Δx at the pulse center, defined as the width of $I(x, z; 0)$, is the inverse of the spatial bandwidth Δk_x .

It is useful to consider the narrowband paraxial limit ($\Delta k_x \ll k_0$ and $\Delta\omega \ll \omega_0$), whereupon the spectral projection of the conic section onto the $(k_x, \frac{\omega}{c})$ -plane can be approximated by a parabola $\frac{\Omega(k_x)}{\omega_0} = \frac{1}{1 - \cot \theta} \frac{k_x^2}{2k_0^2}$ [35]. As such, the spatial and temporal bandwidths are related through

$$\frac{\Delta\omega}{\omega_0} = \frac{1}{|1 - \cot \theta|} \frac{(\Delta k_x)^2}{2k_0^2}; \quad (4)$$

i.e., $\Delta\omega \propto (\Delta k_x)^2$. The proportionality constant between $\Delta\omega$ and $(\Delta k_x)^2$ depends sensitively on the spectral tilt angle θ . When $\theta \rightarrow 45^\circ$ and $\tilde{v} \rightarrow c$, the proportionality constant is large, so that only a small spatial bandwidth Δk_x is required to accommodate a given temporal bandwidth $\Delta\omega$. However, ultraslow ST wave packets $\tilde{v} \ll c$ require $\theta \rightarrow 0^\circ$, in which case the proportionality constant is extremely small and a larger Δk_x is required for the same $\Delta\omega$. For example, with respect to a ST wave packet having $\theta = 44^\circ$ ($\tilde{v} = 0.97c$), reducing the spectral tilt angle to $\theta = 4^\circ$ ($\tilde{v} = 0.07c$) requires increasing Δk_x by a factor of ≈ 19 for the same $\Delta\omega$.

We are now in a position to elucidate our proposed concept of spectral recycling. Spectral recycling aims to *reduce* the separation between the spectral projection of the ST wave packet onto the $(k_z, \frac{\omega}{c})$ -plane and the light-line, which *reduces* the maximum k_x and hence maintains a low numerical aperture despite increase in the temporal bandwidth. To reduce the spatial bandwidth Δk_x of the ST wave packet associated with a fixed temporal bandwidth $\Delta\omega$, we ‘reuse’ the spatial frequencies, or ‘recycle’ them. That is, instead of each k_x being assigned to a single unique temporal frequency ω , each k_x is associated with N distinct and widely separated temporal frequencies: $\omega_1, \omega_2, \dots, \omega_N$. Consider a non-recycled ST wave packet of temporal bandwidth $\Delta\omega$ starting at ω_0 with an associated spatial bandwidth Δk_x . Its spectrally recycled counterpart has the same total temporal bandwidth $\Delta\omega$, but is segmented into N sub-bandwidths $\Delta\omega_n$ starting at distinct frequencies $\omega_{0,n}$, $n = 1, 2, \dots, N$, which are selected such that the associated spatial bandwidths $(\Delta k_x)_n$ are all equal $(\Delta k_x)_n = \Delta k'_x < \Delta k_x$. That is, the spatial bandwidth of the spectrally recycled ST

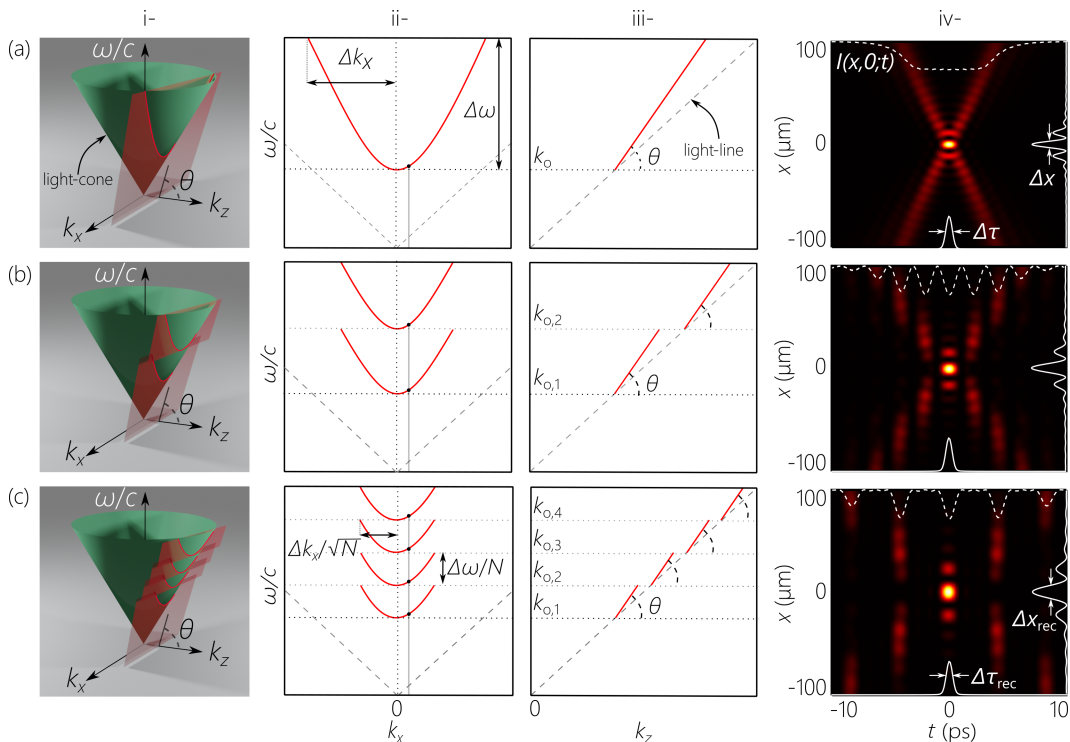


FIG. 1. Concept of spectrally recycled ST wave packets. (a) A ST wave packet with a spectral tilt angle $\theta = 60^\circ$. (b) A spectrally recycled ST wave packet with $N = 2$ and (c) with $N = 4$. Note that the spectral bandwidth Δk_x (and thus the numerical aperture of the optical system) is reduced as N increases for the same temporal bandwidth $\Delta\omega$. i- Three-dimensional representation of the spatio-temporal spectral support of the ST wave packet on the surface of the light-cone in $(k_x, k_z, \frac{\omega}{c})$ space. ii- Spectral projection onto the $(k_x, \frac{\omega}{c})$ -plane, and (iii) onto the $(k_z, \frac{\omega}{c})$ -plane. Spectral recycling entails that each k_x is associated with N distinct temporal frequencies. iv- Spatio-temporal intensity profile $I(x, z; t)$ calculated at a fixed axial plane $z=0$ using $\lambda_0=800$ nm and a temporal bandwidth $\Delta\lambda=2$ nm. We plot along the bottom of the panel in (iv) as a solid white curve the temporal pulse profile at the beam center $I(0, 0; t)$ as recorded by a point detector; we plot along the top of the panel as a dashed curve the spatially averaged temporal profile $\int dx I(x, 0; t)$ as recorded by a ‘bucket’ detector; and on the right we plot as a solid white curve the spatial profile at the center of the pulse $I(x, 0; 0)$. The spatial width Δx of $I(x, 0; 0)$ increases with spectral recycling, but the temporal width $\Delta\tau$ of $I(0, 0; t)$ remains fixed.

wave packet is less than that of its non-recycled counterpart.

This concept is illustrated via two examples depicted in Fig. 1(b,c). In Fig. 1(b), we show a spectrally recycled ST wave packet with $N = 2$ having the same temporal bandwidth as that of the non-recycled ST wave packet in Fig. 1(a). The spatio-temporal spectrum results from the intersection of *two* spectral planes $\omega - \omega_{o,n} = (k_z - k_{o,n})c \tan \theta$ with the light-cone [Fig. 1(b)-i], $k_{o,n} = \omega_{o,n}/c$, $n = 1, 2$, such that the sub-bandwidths are staggered with no spectral gaps [Fig. 1(b)-ii]. The spatial spectra associated with these two sub-bandwidths in the $(k_x, \frac{\omega}{c})$ -plane are both centered at $k_x = 0$, and recycling the use of the spatial frequencies results in each k_x being now associated with *two* temporal frequencies ω (one belonging to each sub-bandwidth) – rather than to one ω as in the non-recycled ST wave packet. Consequently, the spatial bandwidth of the spectrally recycled ST wave packet $\Delta k'_x$ is smaller than that of its non-recycled counterpart despite having the same temporal

bandwidth $\Delta\omega$. A further example illustrates the concept of spectral recycling for the case $N = 4$ as shown in Fig. 1(c). The sub-bandwidths $\Delta\omega_n$ and the associated fixed spatial bandwidth $\Delta k'_x$ are smaller than those for $N = 1$, and each k_x is recycled by associating it with 4 distinct temporal frequencies ω .

In general, holding the recycled spatial spectrum $\Delta k'_x$ fixed necessitates selecting unequal sub-bandwidths $\Delta\omega_n$ because $\Delta\omega_n$ is inversely proportional to $\omega_{o,n}$ for fixed $\Delta k'_x$ as seen in Eq. 4. Consequently, the separations between the distinct temporal frequencies $\omega_1, \omega_2, \dots, \omega_N$ associated with a particular spatial frequency k_x are also unequal. Within the paraxial approximation used in Eq. 4, we have $\omega_n - \omega_{n-1} = (\omega_{o,n} - \omega_{o,n-1})(1 - \Omega_{n-1}(k_x)/\omega_{o,n})$. Only for small bandwidths is $\omega_n - \omega_{n-1} = \omega_{o,n} - \omega_{o,n-1}$. Indeed, in the narrow bandwidth limit $\Delta\omega \ll \omega_0$, the sub-bandwidths are approximately equal $\Delta\omega_n \approx \frac{\Delta\omega}{N}$, and $\Delta k'_x \approx \frac{\Delta k_x}{\sqrt{N}}$, $\omega_{o,n} \approx \omega_0 \pm (n-1) \frac{\Delta\omega}{N}$. The negative sign corresponds to $\theta < 45^\circ$, whereupon $\omega_{o,N} = \omega_0$; and the positive sign used otherwise, where-

upon $\omega_{o,1} = \omega_o$; examples of the latter case are depicted in Fig. 1(b,c).

It is clear from comparing Fig. 1(a)-iv with Fig. 1(c)-iv that spectral recycling results in added structure to the spatio-temporal intensity profile. To gain insight into these changes, we write the spectrally recycled ST wave packet as

$$E_{\text{rec}}(x, z; t) = \sum_{n=1}^N e^{i(k_{o,n}z - \omega_{o,n}t)} \psi_n(x, z; t), \quad (5)$$

where $\psi_n(x, z; t)$ is the envelope associated with the n^{th} sub-bandwidth,

$$\psi_n(x, z; t) = \int_{\Delta\omega_n} dk_x \tilde{\psi}_n(k_x) e^{ik_x x} e^{-i(\omega(k_x) - \omega_{o,n})(t - z/\tilde{v})}. \quad (6)$$

Note that $\psi_n(x, z; t) = \psi_n(x, 0; t - z/\tilde{v})$, so that the envelope associated with each sub-bandwidth also propagates rigidly at the same group velocity $\tilde{v} = c \tan \theta$ as its non-recycled counterpart associated with the full temporal bandwidth $\Delta\omega$.

A particularly simple case is that of a narrowband wave packet whereupon $\Delta\omega_n \approx \frac{\Delta\omega}{N}$, and the associated envelopes $\psi_n(x, z; t)$ are thus almost identical, $\psi_n(x, z; t) \approx \psi_1(x, z; t)$ for all n , in which case:

$$I_{\text{rec}}(x, z; t) \propto I_1(x, z; t) I_f(z - ct), \quad (7)$$

where $I_1(x, z; t) = |\psi_1(x, z; t)|^2$ and the form factor $I_f(z - ct)$ is the familiar term resulting from a phasor sum,

$$I_f(z - ct) = \frac{\sin^2\left(\frac{\Delta\omega_1}{2} N \left(\frac{z}{c} - t\right)\right)}{\sin^2\left(\frac{\Delta\omega_1}{2} \left(\frac{z}{c} - t\right)\right)}. \quad (8)$$

The spectrally recycled ST wave packet is therefore the product of two envelopes: the first is the ST wave packet envelope $I_1(x, z; t)$ that corresponds to a single sub-bandwidth and the second is the form factor $I_f(z - ct)$ that is independent of x . Temporal walk-off occurs between $I_1(x, z; t)$ that travels at \tilde{v} and $I_f(z - ct)$ that travels at c .

To elucidate the structure of spectrally recycled ST wave packets, we plot first in Fig. 2(a) the spatio-temporal profiles of a non-recycled ST wave packet $I(x, z; t)$ of temporal bandwidth $\Delta\omega$, and the envelope $I_1(x, z; t)$ for a single sub-bandwidth $\Delta\omega_1 \approx \frac{\Delta\omega}{N}$ in Fig. 2(b), whose pulsewidths at the beam center are $\Delta\tau \sim \frac{2\pi}{\Delta\omega}$ and $\Delta\tau_1 \sim \frac{2\pi}{\Delta\omega_1} = N\Delta\tau$, respectively. Similarly, the beam widths at the pulse center are $\Delta x \sim \frac{2\pi}{\Delta k_x}$ and $\Delta x_1 \sim \frac{2\pi}{\Delta k'_x} \sim \sqrt{N}\Delta x < \Delta x$. This is expected because of the smaller spatial and temporal bandwidths associated with $I_1(x, z; t)$ in comparison to those associated with $I(x, z; t)$.

Including the N sub-bandwidths in the spectrally recycled ST wave packet results in multiplication of $I_1(x, z; t)$ by the form factor $I_f(z - ct)$ plotted in Fig. 2(c), resulting in the spatio-temporal intensity profile $I_{\text{rec}}(x, z; t)$ shown

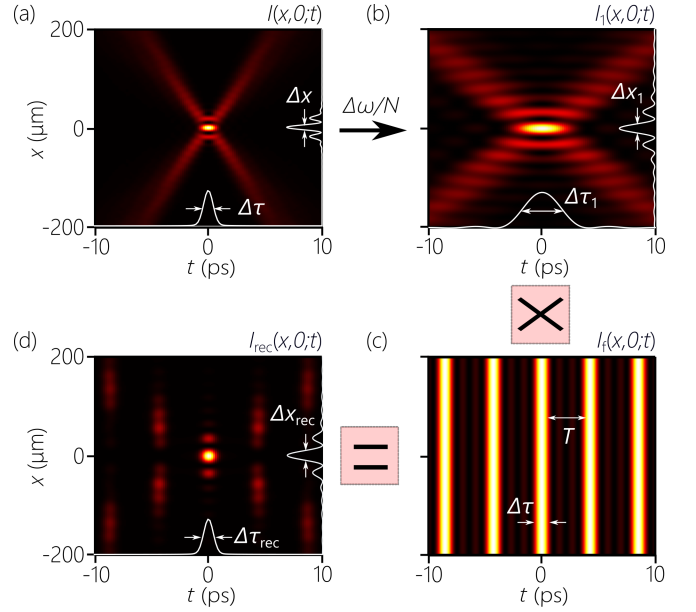


FIG. 2. Change in the spatio-temporal profile $I(x, z; t)$ at a fixed axial plane $z=0$ as a result of spectral recycling. (a) The spatio-temporal intensity profile $I(x, 0; t)$ for a non-recycled ST wave packet with spectral tilt angle $\theta=40^\circ$ and temporal bandwidth $\Delta\lambda=2$ nm. (b) Spatio-temporal intensity profile $I_1(x, 0; t)$ for a ST wave packet corresponding to a *single* sub-bandwidth $\Delta\omega_1$ after spectrally recycling the ST wave packet in (a) with $N=4$; the temporal bandwidth is $\Delta\lambda/N=0.5$ nm. (c) The spatio-temporal intensity of the form-factor $I_f(z - ct)$ ensuing from the process of spectral recycling (Eq. 8). (d) The spatio-temporal intensity profile $I_{\text{rec}}(x, 0; t)$ for a spectrally recycled ST wave packet with $N=4$ corresponding to the wave packet in (a), and resulting from multiplying the profiles in (b) and (c). The spatial width has increased $\Delta x_{\text{rec}} > \Delta x$, but the temporal width remains constant $\Delta\tau = \Delta\tau_{\text{rec}}$.

in Fig. 2(d), where the periodic structure of $I_f(z - ct)$ modulates $I_{\text{rec}}(x, z; t)$. The pulsewidth at the beam center of the spectrally recycled wave packet is $\Delta\tau_{\text{rec}} \sim \frac{4\pi}{N\Delta\omega_1} = \Delta\tau$, similar to that of the non-recycled ST wave packet $I(x, z; t)$. Nevertheless, because $I_f(z - ct)$ is independent of x , the beam width at the pulse center remains larger than that for $I(x, z; t)$, $\Delta x_{\text{rec}} = \Delta x_1 < \Delta x$; indeed, $\Delta x_1 \sim \sqrt{N}\Delta x$. We have thus retained the narrow temporal width associated with the full temporal bandwidth, while increasing the beam transverse width and thus reducing the associated numerical aperture. Increasing N increases the separation $T = N\frac{2\pi}{\Delta\omega}$ between the discrete features in the spatio-temporal profile, while decreasing the width of these features.

We can draw several conclusions from this theoretical analysis. First, spectral recycling does *not* affect the critical properties of a ST wave packet, including its propagation invariance and its group velocity \tilde{v} . Second, the temporal linewidth of the pulse at the beam center of the spectrally recycled ST wave packet is similar to that of its non-recycled counterpart, while maintaining a larger

beam width at the pulse center. This indicates that the proportionality between the spatial and temporal bandwidths has been modified *without* changing the spectral tilt angle θ . We now proceed to verify experimentally the concept of spectrally recycling ST wave packets and to validate these theoretical predictions concerning their properties.

III. EXPERIMENTAL CONFIGURATION

The setup utilized for our proof-of-principle demonstration of spectral recycling is similar to that used previously for synthesizing ST wave packets [30, 33, 46]. Beginning with ~ 100 -fs pulses from a modelocked Ti:sapphire laser (Tsunami; Spectra Physics) of central wavelength ~ 800 nm, the pulse spectrum is spread via a diffraction grating and collimated by a cylindrical lens before impinging on a two-dimensional, reflective, phase-only spatial light modulator (SLM; Hamamatsu X10468-02). The SLM imparts a phase distribution to the wave front designed to associate each wavelength λ with a prescribed spatial frequency k_x in order to satisfy the constraint in Eq. 2. The retro-reflected field is reconstituted into a ST wave packet at the diffraction grating. We record the spatio-temporal spectrum $|\tilde{\psi}(k_x, \lambda)|^2$, the spatio-temporal profile of the ST wave packets $I(x, z; \tau)$ at different axial planes z , which allows us to assess the group velocity \tilde{v} , in addition to the axial evolution of the time-averaged intensity $I(x, z)$.

We consider three ST wave packets having spectral tilt angles $\theta = 30^\circ$ (subluminal $\tilde{v} = 0.58c$), $\theta = 70^\circ$ (superluminal, $\tilde{v} = 2.75c$) and $\theta = 110^\circ$ (negative- \tilde{v} , $\tilde{v} = -2.75c$). In each case we carry out the measurements for different extents of spectral recycling: $N = 1$ (non-recycled, $\Delta\lambda = 2$ nm), $N = 2$ ($\Delta\lambda_n \approx 1$ nm, $n = 1, 2$), and $N = 4$ ($\Delta\lambda_n \approx 0.5$ nm, $n = 1, 2, 3, 4$).

IV. MEASUREMENTS RESULTS

The spatio-temporal spectra for all 9 ST wave packets are plotted in Fig. 3. In each case, we observe that the measured spatio-temporal spectrum $|\tilde{\psi}(k_x, \lambda)|^2$ is divided into N segments all centered at $k_x = 0$. Note the switch in sign of the curvature of the spectral projections onto the $(k_x, \frac{\omega}{c})$ -plane from the subluminal case ($\theta = 30^\circ$) to the superluminal cases ($\theta = 70^\circ$ and 110°). The impact of spectral recycling is particularly clear when examining the spectral projection onto the $(k_x, \frac{\omega}{c})$ -plane, as shown in Fig. 4. Here we see clearly that the spectral projection for the non-recycled ST wave packet extends further away from the light-line (corresponding to larger values of associated k_x) than in its spectrally recycled counterparts. Spectral recycling divides this projection into N sections, and the segments are shifted accordingly along k_x such that the sub-bandwidths are staggered, leaving no spectral gaps. The maximum deviation away from the light-

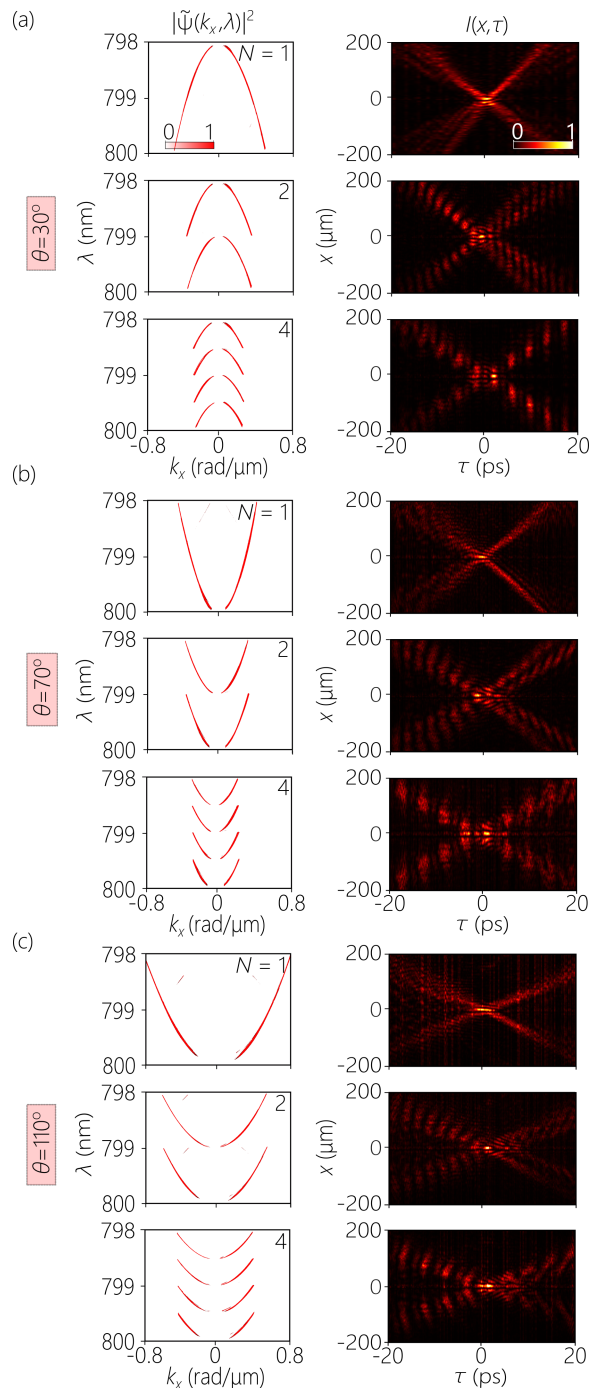


FIG. 3. Measurements of the spatio-temporal spectrum $|\tilde{\psi}(k_x, \lambda)|^2$ (left column) and the spatio-temporal profile $I(x, z; t)$ at a fixed axial plane $z = 10$ mm (right column). (a) The ST wave packet has a spectral tilt angle 30° , (b) $\theta = 70^\circ$, and (c) $\theta = 110^\circ$. In each panel we plot three cases: $N = 1$ (no spectral recycling), $N = 2$, and $N = 4$.

line is reduced as N increases, indicating a reduction in the spatial bandwidth and thus also the numerical aperture. We plot the spatio-temporal profiles $I(x, z; t)$ at fixed z for all these cases in Fig. 3. The non-recycled ST

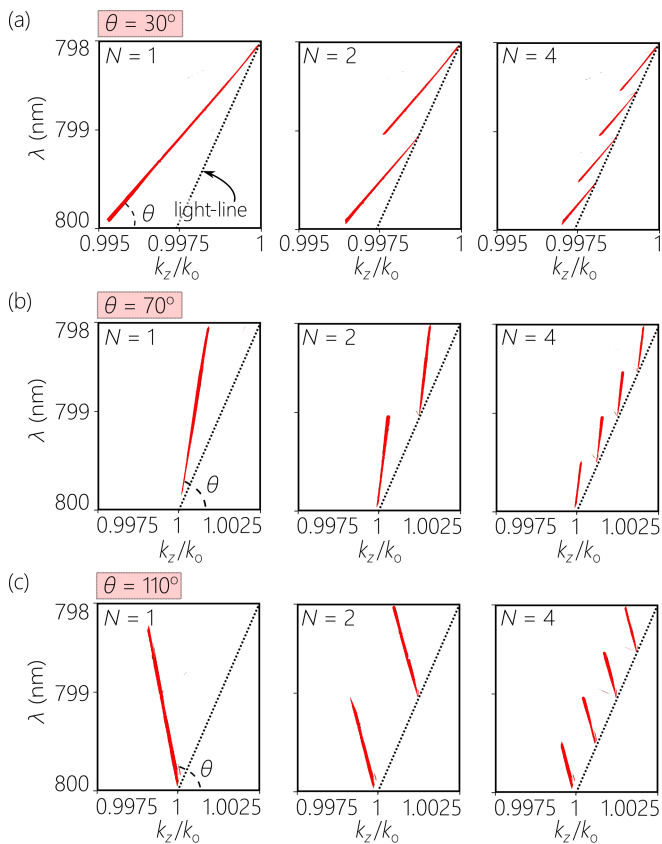


FIG. 4. Measurements of the spectral projections onto the $(k_z, \frac{\omega}{c})$ -plane for (a) a ST wave packet having a spectral tilt angle $\theta = 30^\circ$, (b) $\theta = 70^\circ$, and (c) $\theta = 110^\circ$. In each panel we plot three cases: $N=1$ (no spectral recycling), $N=2$, and $N=4$, corresponding to the 9 cases shown in Fig. 3.

wave packets show the expected characteristic X-shape, while those of the spectrally recycled counterparts have the overall X-shaped profile modulated by a discretized structure as predicted in Eq. 7 and Eq. 8.

We next proceed to verify that spectral recycling retains the group velocity of the original non-recycled ST wave packet. The slope of the spectral projection onto the $(k_z, \frac{\omega}{c})$ -plane (that is, the spectral tilt angle θ) determines the group velocity. This conclusion has been well-established for non-recycled ST wave packets ($N=1$) [32, 33, 46] and is expected to extend to their spectrally recycled counterparts. To assess the validity of this conception, we measured the group velocity directly using the approach we developed in [32, 34]. This requires measuring the relative group delay between the ST wave packet traveling at \tilde{v} and a reference laser pulse traveling at c , after both wave packets traverse the same distance. From this measured relative group delay we estimate \tilde{v} . In Fig. 5 we plot the measured \tilde{v} while varying the spectral tilt angle θ for different extents of spectral recycling ($N=1, 2, 4$, and 6). All the measurements follow the same theoretical curve $\tilde{v} = c \tan \theta$ independently of N ,

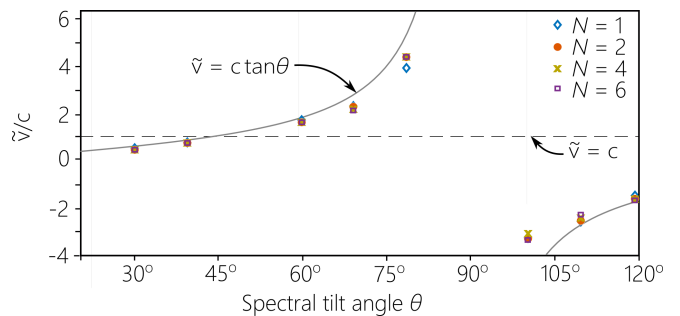


FIG. 5. Measurements of the group velocity \tilde{v} of ST wave packets while varying the spectral tilt angle θ . The solid curve is the theoretical expectation for a non-recycled ST wave packet $\tilde{v} = c \tan \theta$. The points correspond to measurements for non-recycled ($N=1$) and spectrally recycled ST wave packets ($N=2, 4$, and 6). All the data points lie along the theoretical curve, indicating that spectral recycling does not affect \tilde{v} .

thereby confirming that spectral recycling does *not* impact the group velocity of the ST wave packet.

We finally demonstrate that circumventing the usual proportionality between the spatial and temporal bandwidths, Δk_x and $\Delta \omega$, respectively, through spectral recycling, facilitates for the synthesis of ultraslow ST wave packets. Previously, the slowest subluminal ST we prepared corresponded to $\theta = 10^\circ$ ($\tilde{v} \approx c/5.7$) [51]. In Fig. 6 we plot the measurement results for the synthesis of a ST wave packet with $\theta = 4^\circ$ ($\tilde{v} \approx c/14.3$). Here, making use of a temporal bandwidth of $\Delta \lambda \approx 2$ nm at $\lambda_0 = 800$ nm, synthesizing a ST wave packet with $\theta = 4^\circ$ requires a large spatial bandwidth $\Delta k_x \approx 0.26 k_0$, which is prohibitively difficult to produce. Instead, through spectral recycling with $N=16$, the spatial bandwidth required is reduced to $\Delta k_x \approx 0.064 k_0$, which is that corresponding to a non-recycled ST wave packet having $\tilde{v} = c/2$ and the same full temporal bandwidth $\Delta \lambda \approx 2$ nm. In Fig. 6(a) we plot the measured spectral projection onto the (k_x, λ) and (k_z, λ) planes, which show clearly the spectrally recycled structure of the spatio-temporal spectrum. We plot in Fig. 6(b) the spatio-temporal intensity profile $I_{\text{rec}}(x, z; t)$.

V. DISCUSSION

A final characteristic of the spectrally recycled ST wave packets to consider is their time-averaged intensity $I(x, z) = \int dt I(x, z; t)$, that is captured by a slow detector such as a CCD camera. Because the form-factor $I_f(z - ct)$ is independent of x , the time-averaged intensity of the spectrally recycled ST wave packet $I_{\text{rec}}(x, z)$ is diffraction-free with width Δx_1 (corresponding to the spatial bandwidth $\Delta k'_x$) of a single sub-bandwidth.

The question remains whether spectral recycling affects the maximum propagation distance L_{max} of a ST wave packet, defined as the propagation distance after

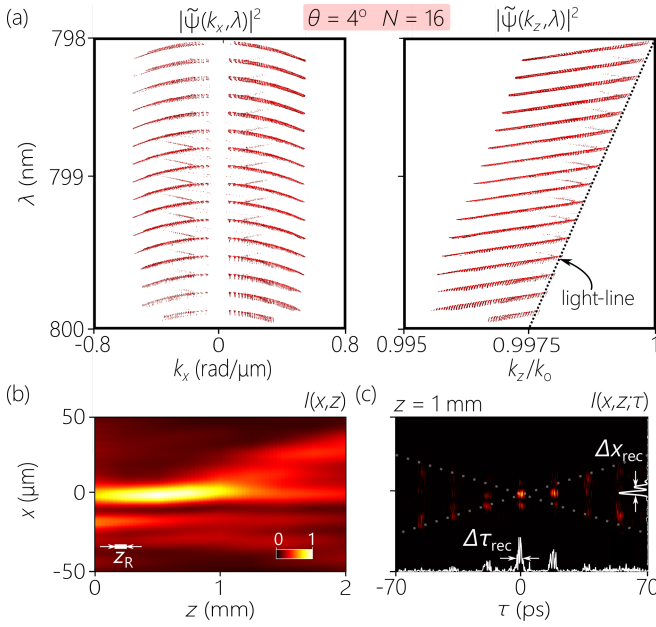


FIG. 6. Measurement of an extreme subluminal wave packet at $\theta = 4^\circ$ ($\tilde{v} = c/14.3$). The ST wave packet is spectrally recycled with $N = 16$. (a) The measured spatio-temporal spectra $|\tilde{\psi}(k_x, \lambda)|^2$ and $|\tilde{\psi}(k_z, \lambda)|^2$. (b) The time-averaged intensity $I(x, z)$. (c) The spatio-temporal profile $I(x, z; \tau)$ measured at the axial plane $z = 1$ mm. The measured pulse width at $x = 0$ is $\Delta\tau_{\text{rec}} \approx 3$ ps. The dotted white lines are guides for the eye to discern the X-shape of $I(x, z; \tau)$.

which the on-axis intensity drops to half its initial value $I(0, L_{\text{max}}) = 0.5I(0, 0)$. We have recently shown that L_{max} for a non-recycled ST wave packet is

$$L_{\text{max}} \sim \frac{c}{\delta\omega} \frac{1}{|1 - \cot \theta|}, \quad (9)$$

where $\delta\omega$ is the ‘spectral uncertainty’, which is the unavoidable fuzziness in the association between any k_x and its assigned ω [33]. An ideal delta function correlation in the spatio-temporal spectrum $\tilde{\psi}(k_x, \Omega) \rightarrow \tilde{\psi}(k_x)\delta(\Omega - \Omega(k_x))$ requires infinite energy and cannot be realized in any finite optical arrangement [52, 53]. Instead, in realistic systems [54, 55], $\tilde{\psi}(k_x, \Omega) \rightarrow \tilde{\psi}(k_x)h(\Omega - \Omega(k_x))$, where $h(\Omega)$ is a narrow spectral function of width $\delta\omega$, which then determines L_{max} [33, 56]. Counter-intuitively, L_{max} is *not* related to the relative measure $\frac{\Delta\omega}{\delta\omega}$ between the full bandwidth $\Delta\omega$ and the spectral uncertainty $\delta\omega$. Instead, L_{max} is dictated by the absolute value of $\delta\omega$ independently of $\Delta\omega$. This suggests that L_{max} is also unaffected by spectral recycling as long as the recycling process does not impact $\delta\omega$. Measurements support this suggestion as shown in Fig. 7(a) where we plot L_{max} while varying θ for ST wave packets of different levels of spectral recycling N . The measurements all lie along the theoretical expectation for L_{max} in Eq. 9 for non-recycled and recycled ST wave packets independently of N . This is further highlighted in Fig. 7(b) where we plot $I_{\text{rec}}(x, z)$ for a wave

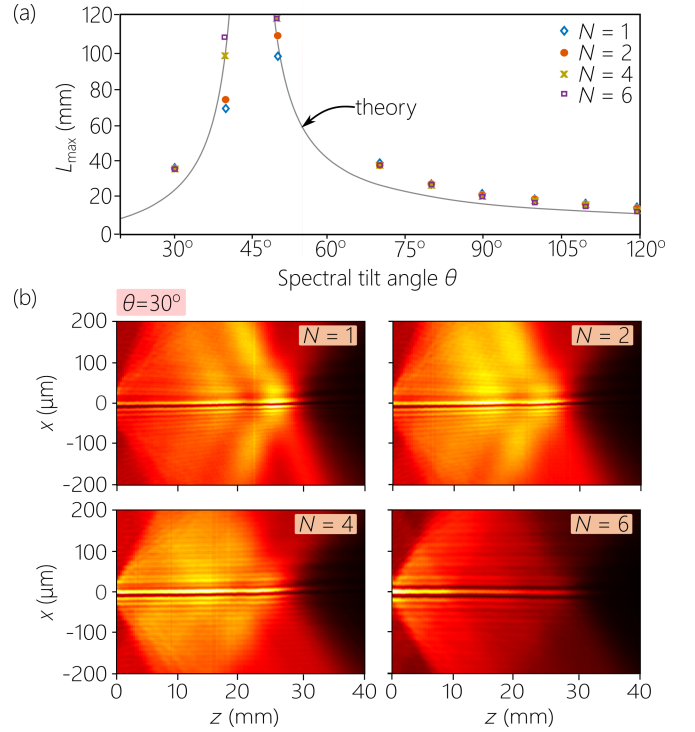


FIG. 7. Invariance of the propagation distance L_{max} with respect to spectral recycling. (a) Measured L_{max} of spectrally recycled ST wave packet with $N = 1, 2, 4$, and 6 . The circles represent data points and the solid curve represents the theoretical expectation for a non-recycled ST wave packet (Eq. 9) over a range of spectral tilt angles $\theta = 30^\circ - 120^\circ$. (b) The axial evolution of the time-averaged intensity $I(x, z)$ of spectrally recycled ST wave packets at $\theta = 30^\circ$ for $N = 1, 2, 4$, and 6 .

packet with $\theta = 30^\circ$ ($\tilde{v} \approx 0.58c$) for $N = 1, 2, 4$, and 6 . The propagation distance L_{max} remains constant despite the increase in transverse width Δx_1 with N . Furthermore, the measured time-averaged intensity $I_{\text{rec}}(x, z)$ for the ultraslow ST wave packet in Fig. 6(c) also satisfies the theoretical limit. These results confirm that spectral recycling does not impact L_{max} negatively.

VI. CONCLUSIONS

In conclusion, we have proposed and demonstrated a technique we have called ‘spectral recycling’ that helps circumvent the proportionality between spatial and temporal bandwidths intrinsic to ST wave packets. In contrast to traditional pulsed optical beams where the spatial and temporal degrees of freedom are more-or-less independent, each spatial frequency k_x in a ST wave packet is typically associated with a single temporal frequency ω (or wavelength). The spectral recycling strategy ‘reuses’ or ‘recycles’ each spatial frequency k_x by associating it with N distinct and well-separated temporal frequencies $\omega_1, \omega_2, \dots, \omega_N$ to maintain a fixed spatial bandwidth in-

dependently of an increasing temporal bandwidth. We confirmed experimentally that spectral recycling even up to $N = 16$ does *not* affect the unique characteristics of a ST wave packet: its propagation invariance, its group velocity \tilde{v} , and its maximum propagation distance L_{\max} all remain intact. This strategy facilitates the synthesis of ultraslow ST wave packets in free space without exorbitant increase in the required numerical aperture. Indeed, we demonstrated here $\tilde{v} = c/14.3$ with the same numerical aperture associated with $\tilde{v} = c/2$. It is expected that spectral recycling will enable the utilization of broadband optical sources in the synthesis of ST wave packets, while maintaining a low numerical aperture. This will be particularly useful in application in which a broadband ST

wave packet is required, such as in omni-resonant coupling to planar cavities [57, 58], nonlinear optics, and laser-plasma interactions. Finally, it would also be interesting to examine whether spectral recycling can benefit another recently developed class of optical wave packets having controllable group velocity known as a ‘flying focus’ [59–61].

ACKNOWLEDGMENTS

This work was funded by the U.S. Office of Naval Research (ONR) under contract N00014-17-1-2458, and ONR MURI contract N00014-20-1-2789.

-
- [1] J. N. Brittingham, Focus wave modes in homogeneous Maxwell’s equations: Transverse electric mode, *J. Appl. Phys.* **54**, 1179 (1983).
 - [2] P. Saari and K. Reivelt, Evidence of X-shaped propagation-invariant localized light waves, *Phys. Rev. Lett.* **79**, 4135 (1997).
 - [3] J. Salo, J. Fagerholm, A. T. Friberg, and M. M. Salomaa, Unified description of nondiffracting X and Y waves, *Phys. Rev. E* **62**, 4261 (2000).
 - [4] K. Reivelt and P. Saari, Localized wave solutions of the scalar homogeneous wave equation and their optical implementation, arxiv:physics/0309079 (2003).
 - [5] D. N. Christodoulides, N. K. Efremidis, P. Di Trapani, and B. A. Malomed, Bessel X waves in two- and three-dimensional bidispersive optical systems, *Opt. Lett.* **29**, 1446 (2004).
 - [6] A. P. Kiselev, Localized light waves: Paraxial and exact solutions of the wave equation (a review), *Opt. Spectrosc.* **102**, 603 (2007).
 - [7] Y. Lahini, E. Frumker, Y. Silberberg, S. Droulias, K. Hizanidis, R. Morandotti, and D. N. Christodoulides, Discrete X-wave formation in nonlinear waveguide arrays, *Phys. Rev. Lett.* **98**, 023901 (2007).
 - [8] H. E. Hernández-Figueroa, E. Recami, and M. Zamboni-Rached, eds., *Localized waves* (Wiley-Interscience, 2008).
 - [9] J. Turunen and A. T. Friberg, Propagation-invariant optical fields, *Prog. Opt.* **54**, 1 (2010).
 - [10] H. E. Hernández-Figueroa, E. Recami, and M. Zamboni-Rached, eds., *Non-diffracting Waves* (Wiley-VCH, 2014).
 - [11] H. E. Kondakci and A. F. Abouraddy, Diffraction-free pulsed optical beams via space-time correlations, *Opt. Express* **24**, 28659 (2016).
 - [12] K. J. Parker and M. A. Alonso, The longitudinal isophase condition and needle pulses, *Opt. Express* **24**, 28669 (2016).
 - [13] M. A. Porras, Gaussian beams diffracting in time, *Opt. Lett.* **42**, 4679 (2017).
 - [14] N. K. Efremidis, Spatiotemporal diffraction-free pulsed beams in free-space of the Airy and Bessel type, *Opt. Lett.* **42**, 5038 (2017).
 - [15] L. J. Wong and I. Kaminer, Abruptly focusing and defocusing needles of light and closed-form electromagnetic wavepackets, *ACS Photon.* **4**, 1131 (2017).
 - [16] L. J. Wong and I. Kaminer, Ultrashort tilted-pulsefront pulses and nonparaxial tilted-phase-front beams, *ACS Photon.* **4**, 2257 (2017).
 - [17] M. A. Porras, Nature, diffraction-free propagation via space-time correlations, and nonlinear generation of time-diffracting light beams, *Phys. Rev. A* **97**, 063803 (2018).
 - [18] L. J. Wong, D. N. Christodoulides, and I. Kaminer, The complex charge paradigm: A new approach for designing electromagnetic wavepackets, *Adv. Sci.* **7**, 1903377 (2020).
 - [19] R. Donnelly and R. Ziolkowski, Designing localized waves, *Proc. R. Soc. Lond. A* **440**, 541 (1993).
 - [20] P. Saari and K. Reivelt, Generation and classification of localized waves by Lorentz transformations in Fourier space, *Phys. Rev. E* **69**, 036612 (2004).
 - [21] S. Longhi, Gaussian pulsed beams with arbitrary speed, *Opt. Express* **12**, 935 (2004).
 - [22] J. Salo and M. M. Salomaa, Diffraction-free pulses at arbitrary speeds, *J. Opt. A* **3**, 366 (2001).
 - [23] I. Alexeev, K. Y. Kim, and H. M. Milchberg, Measurement of the superluminal group velocity of an ultrashort Bessel beam pulse, *Phys. Rev. Lett.* **88**, 073901 (2002).
 - [24] C. J. Zapata-Rodríguez and M. A. Porras, X-wave bullets with negative group velocity in vacuum, *Opt. Lett.* **31**, 3532 (2006).
 - [25] H. Valtna, K. Reivelt, and P. Saari, Methods for generating wideband localized waves of superluminal group velocity, *Opt. Commun.* **278**, 1 (2007).
 - [26] M. Zamboni-Rached and E. Recami, Subluminal wave bullets: Exact localized subluminal solutions to the wave equations, *Phys. Rev. A* **77**, 033824 (2008).
 - [27] F. Bonaretti, D. Faccio, M. Clerici, J. Biegert, and P. Di Trapani, Spatiotemporal amplitude and phase retrieval of Bessel-X pulses using a Hartmann-Shack sensor, *Opt. Express* **17**, 9804 (2009).
 - [28] P. Bowlan, H. Valtna-Lukner, M. Löhmus, P. Piskarv, P. Saari, and R. Trebino, Measuring the spatiotemporal field of ultrashort Bessel-X pulses, *Opt. Lett.* **34**, 2276 (2009).
 - [29] K. B. Kuntz, B. Braverman, S. H. Youn, M. Lobino, E. M. Pessina, and A. I. Lvovsky, Spatial and temporal characterization of a Bessel beam produced using a conical mirror, *Phys. Rev. A* **79**, 043802 (2009).

- [30] H. E. Kondakci and A. F. Abouraddy, Diffraction-free space-time beams, *Nat. Photon.* **11**, 733 (2017).
- [31] M. Yessenov, B. Bhaduri, H. E. Kondakci, and A. F. Abouraddy, Weaving the rainbow: Space-time optical wave packets, *Opt. Photon. News* **30**, 34 (2019).
- [32] H. E. Kondakci and A. F. Abouraddy, Optical space-time wave packets of arbitrary group velocity in free space, *Nat. Commun.* **10**, 929 (2019).
- [33] M. Yessenov, B. Bhaduri, L. Mach, D. Mardani, H. E. Kondakci, M. A. Alonso, G. A. Atia, and A. F. Abouraddy, What is the maximum differential group delay achievable by a space-time wave packet in free space?, *Opt. Express* **27**, 12443 (2019).
- [34] B. Bhaduri, M. Yessenov, and A. F. Abouraddy, Space-time wave packets that travel in optical materials at the speed of light in vacuum, *Optica* **6**, 139 (2019).
- [35] B. Bhaduri, M. Yessenov, and A. F. Abouraddy, Anomalous refraction of optical spacetime wave packets, *Nat. Photon.* **14**, 416 (2020).
- [36] A. Shiri, M. Yessenov, S. Webster, K. L. Schepler, and A. F. Abouraddy, Hybrid guided space-time optical modes in unpatterned films, arXiv:2001.01991 (2020).
- [37] K. L. Schepler, M. Yessenov, Y. Zhiyenbayev, and A. F. Abouraddy, Space-time surface plasmon polaritons: A new propagation-invariant surface wave packet, *ACS Photonics* 10.1021/acsp Photonics.0c00293 (2020).
- [38] M. Yessenov and A. F. Abouraddy, Accelerating and decelerating space-time optical wave packets in free space, arXiv:2004.00380 (2020).
- [39] H. E. Kondakci and A. F. Abouraddy, Airy wavepackets accelerating in space-time, *Phys. Rev. Lett.* **120**, 163901 (2018).
- [40] H. E. Kondakci and A. F. Abouraddy, Self-healing of space-time light sheets, *Opt. Lett.* **43**, 3830 (2018).
- [41] M. Yessenov, L. A. Hall, S. A. Ponomarenko, and A. F. Abouraddy, Veiled talbot effect, arXiv preprint arXiv:2004.04875 (2020).
- [42] M. Yessenov, B. Bhaduri, H. E. Kondakci, M. Meem, R. Menon, and A. F. Abouraddy, Diffraction-free broadband incoherent space-time fields, *Optica* **6**, 598 (2019).
- [43] M. Yessenov and A. F. Abouraddy, Changing the speed of optical coherence in free space, *Opt. Lett.* **44**, 5125 (2019).
- [44] H. E. Kondakci, M. Yessenov, M. Meem, D. Reyes, D. Thul, S. R. Fairchild, M. Richardson, R. Menon, and A. F. Abouraddy, Synthesizing broadband propagation-invariant space-time wave packets using transmissive phase plates, *Opt. Express* **26**, 13628 (2018).
- [45] B. Bhaduri, M. Yessenov, D. Reyes, J. Pena, M. Meem, S. R. Fairchild, R. Menon, M. C. Richardson, and A. F. Abouraddy, Broadband space-time wave packets propagating for 70 m, *Opt. Lett.* **44**, 2073 (2019).
- [46] M. Yessenov, B. Bhaduri, H. E. Kondakci, and A. F. Abouraddy, Classification of propagation-invariant space-time light-sheets in free space: Theory and experiments, *Phys. Rev. A* **99**, 023856 (2019).
- [47] A. M. Shaarawi and I. M. Besieris, Relativistic causality and superluminal signalling using X-shaped localized waves, *J. Phys. A* **33**, 7255 (2000).
- [48] P. Saari, Reexamination of group velocities of structured light pulses, *Phys. Rev. A* **97**, 063824 (2018).
- [49] P. Saari, O. Rebane, and I. Besieris, Reexamination of energy flow velocities of non-diffracting localized waves, *Phys. Rev. A* **100**, 013849 (2019).
- [50] B. E. A. Saleh and M. C. Teich, *Fundamentals of Photonics* (Wiley, 2019).
- [51] M. Yessenov, B. Bhaduri, P. J. Delfyett, and A. F. Abouraddy, Free-space optical delay line using space-time wave packets, arXiv:1910.05616 (2019).
- [52] A. Sezginer, A general formulation of focus wave modes, *J. Appl. Phys.* **57**, 678 (1985).
- [53] R. W. Ziolkowski, Exact solutions of the wave equation with complex source locations, *J. Math. Phys.* **26**, 861 (1985).
- [54] R. W. Ziolkowski, I. M. Besieris, and A. M. Shaarawi, Aperture realizations of exact solutions to homogeneous-wave equations, *J. Opt. Soc. Am. A* **10**, 75 (1993).
- [55] M. Zamboni-Rached, Analytical expressions for the longitudinal evolution of nondiffracting pulses truncated by finite apertures, *J. Opt. Soc. Am. A* **23**, 2166 (2006).
- [56] H. E. Kondakci, M. A. Alonso, and A. F. Abouraddy, Classical entanglement underpins the propagation invariance of space-time wave packets, *Opt. Lett.* **44**, 2645 (2019).
- [57] S. Shabahang, H. E. Kondakci, M. L. Villinger, J. D. Perlstein, A. El Halawany, and A. F. Abouraddy, Omni-resonant optical micro-cavity, *Sci. Rep.* **7**, 10336 (2017).
- [58] A. Shiri, M. Yessenov, R. Aravindakshan, and A. F. Abouraddy, Omni-resonant space-time wave packets, *Opt. Lett.* **45** (2020).
- [59] A. Sainte-Marie, O. Gobert, and F. Quéré, Controlling the velocity of ultrashort light pulses in vacuum through spatio-temporal couplings, *Optica* **4**, 1298 (2017).
- [60] D. H. Froula, D. Turnbull, A. S. Davies, T. J. Kessler, D. Haberberger, J. P. Palastro, S.-W. Bahk, I. A. Begishev, R. Boni, S. Bucht, J. Katz, and J. L. Shaw, Spatiotemporal control of laser intensity, *Nat. Photon.* **12**, 262 (2018).
- [61] S. W. Jolly, O. Gobert, A. Jeandet, and F. Quéré, Controlling the velocity of a femtosecond laser pulse using refractive lenses, *Opt. Express* **28**, 4888 (2020).